TIDAL COUPLING WITH THE LOWER ATMOSPHERE
(Invited Review)

Jeffrey M. Forbes
Department of Electrical, Computer, and Systems Engineering
Boston University, Boston, MA 02215

1. INTRODUCTION

The purpose of this paper is to review the various ways in which propagating tidal components excited in the mesophere and below affect the structure of the thermosphere and ionosphere above 100 km. Dynamo effects are not treated here, as they will be addressed separately in the paper by A. D. Richmond.

We begin by examining the physical processes affecting the propagation of upward propagating tides, and how they are interrelated in the context of a numerical model. Propagating diurnal and semidiurnal tides which reach thermospheric heights are excited *primarily* by insolation absorption by tropospheric water vapor (0-15 km) and stratospheric/mesospheric ozone (40-60 km), respectively. Simulation of these oscillations requires consideration of mean zonal winds and meridional temperature gradients, and the damping effects of turbulent and molecular dissipation, radiative cooling, and ion drag. These effects must be considered on a spherical rotating atmosphere extending from the ground to above 300 km, as they are in the model developed by Forbes (1982 a, b) depicted schematically in Figure 1.

2. WINDS AND TEMPERATURES

Figure 2 illustrates amplitudes and phase vertical structures at $0°$, $18°$, $42°$, and $60°$ latitude for the solar diurnal westerly wind at equinox from the Forbes model. In-situ EUV excitation above 90 km is included in these simulations. The following features are worth noting:

(1) Below 100 km at low latitudes the exponential amplitude growth and phase progression ($\lambda_z \approx 30$ km) with height are characteristic of the (1, 1) diurnal propagating tide. The (1, 1) mode attains its peak amplitudes near 110 km and decays rapidly above this height due to molecular dissipation.

(2) Below 100 km at high latitudes the relative absence of amplitude growth and phase progression with height is indicative of the (1, -2) trapped mode. Superposition of the (1, 1) and (1, -2) modes accounts for the illustrated changes in vertical structure of the diurnal tidal winds and temperatures.

(3) Amplitudes and phases of u, v, and δT are asymptotic to constant values above 200 km. This behavior is consistent with the dominance of diffusion in the upper thermosphere, and with the condition that there be no sources of heat or momentum in the upper thermosphere.

(4) Diurnal tidal oscillations in the 90-150 km region receive about equal contributions from upward propagating and in situ excited components.

Item (4) is examined in detail in Figure 3 where the *northerly velocity* at 18° latitude is separated into relative contributions due to the (1, 1) propagating tide (predominant below 150 km) and that excited in-situ by EUV and UV solar radiation absorption (predominant above 150 km). Note the transition from a 30-km vertical wavelength phase progression with height below 150 km indicative of the (1, 1) mode to phase and amplitude constancy with height indicative of fast molecular diffusion and in situ excitation.

Figures 4 and 5 illustrate amplitude and phase vertical structures at 0°, 18°, 42°, and 60° latitude for the solar and lunar semidiurnal westerly winds at equinox from the Forbes model. For the solar component the transition to shorter vertical wavelengths between 80 and 100 km, the effects of dissipation on the upward propagating components between 110 and 150 km, and the asymptotic behavior characteristic of the upper thermosphere are clearly illustrated. The upper thermosphere velocity and temperature fields, which typically range between 10-50 m sec^{-1} and 20-40 K with the larger values at low latitudes, originate with about equal weighting from three excitation sources: (1) in situ EUV excitation, (2) ion-drag momentum coupling with the diurnal tidal winds, and (3) upward propagating modes excited below 100 km. Although the lunar gravitational excitation consists of some (2, 4) in addition to the predominant (2, 2) forcing, the excitation of the higher-order (2, 4) and (2, 5) modes are due almost exclusively to mode coupling due to mesospheric mean winds and meridional temperature gradients. Winds (temperatures), in fact, reach amplitudes of order 10-15 m sec^{-1} (10-15 K) in the lower thermosphere, and 5-10 m sec^{-1} (5-10 K) in the upper thermosphere, and may thus account for a significant portion of day-to-day variability reported in measurements of the solar semidiurnal tide.

The joint presence of molecular viscosity, thermal conductivity, anisotropic ion drag, and rotation on a sphere renders the viscid tidal equations inseparable with respect to height and latitude, whereas in an inviscid atmosphere where the background temperature is independent of latitude the equations are separable, and classical tidal theory applies. In classical tidal theory the eigensolutions (Hough functions) of Laplace's tidal equation define the horizontal structures of each mode, and the eigenvalues (equivalent depths) fix each mode's vertical structure. Thus, besides alteration of the vertical tidal structures from exponential growth (for propagating tides) or decay (for trapped tides) to asymptotically constant solutions in the upper thermosphere, the region where χ, the ratio of the wave period to the dissipative time scale, approaches unity is also characterized by a transition from tidal solutions that are separable with respect to height and latitude to one in which vertical structures for a particular 'modal extension' into the thermosphere vary with height. This behavior is illustrated in Figures 7 and 8, which depict the horizontal shapes of the (2, 2) and (2, 4) Hough mode extensions (HME) of the semidiurnal temperature oscillation at various heights. Note that the node at 15° latitude for (2, 4) disappears and the (2, 2) horizontal shape broadens considerably at progressively greater heights in the thermosphere.

An illustration of how upward-propagating tides affect the local-time structure of the thermosphere is illustrated in Figure 9, taken from Garrett and Forbes (1978). These authors superimposed in-situ diurnal simulations with theoretical semidiurnal 'Hough mode extensions' calibrated to observational data. Note the high degree of structure exhibited below 200 km. The hour of maximum amplitude shifts to earlier times with increasing altitude, indicating the presence of upward propagation waves. A 12-hour period is particularly evident below 150 km.

At solar minimum, the upward propagating components can be expected to exert a greater influence on thermospheric structure, due to the relatively smaller contribution from in-situ EUV sources. An example of how this influence can be reflected in midlatitude exospheric temperatures is illustrated in Figures 10 and 11, where temperatures measured at Millstone Hill during 1974 (SSMIN) and 1980 (SSMAX) are depicted. Note the predominance of a diurnal component at SSMAX whereas the SSMIN curve exhibits structure containing semidiurnal and terdiurnal components.

Another manifestation of upward propagating tides occurs via the nonlinear coupling between the semidiurnal thermospheric oscillation (which originates via in-situ as well as lower atmosphere contributions) and the diurnal variation of ion drag to produce a terdiurnal component to the thermospheric temperature and density, particularly at low latitudes where the coupling is strong. The nonlinear coupling between tidal winds and ion drag has been invoked by Mayr et al (1974) to explain spurious anamalous increases in the equatorial neutral temperature around midnight observed by the NATE experiment on AE-E, as illustrated in Figure 12. The semidiurnal component receives strong contributions from (a) diurnal winds interacting with the diurnal ion drag and (b) upward propagating modes excited by O_3 insolation absorption. The semidiurnal fields interacting with the diurnal component of ion drag, in turn, generate a substantial terdiurnal component. The synthesis of all contributions can yield the signature of a midnight temperature maximum in the upper thermosphere as illustrated in Figure 12.

3. ACCELERATION AND HEATING OF THE LOWER THERMOSPHERE DUE TO DISSIPATING TIDAL WAVES.

In the zonal mean, the atmosphere can be accelerated and heated by the deposition of momentum and thermal energy by the so-called 'eddy' or 'perturbation' motions of the atmosphere. Since gravity wave and tidal amplitudes grow exponentially with height, it has often been suggested that these motions might contribute significantly to the mean momentum and energy budget of the lower thermosphere. These effects enter in the zonal mean momentum equation as a divergence of the eastward eddy momentum flux:

$$\overline{F}_u = \frac{1}{a\cos^2\phi} \frac{\partial}{\partial\phi} (\overline{u'v'}\cos^2\phi) - \frac{1}{p} \frac{\partial}{\partial z} p \overline{u'w'}$$

and in the thermal energy equation as a divergence of the thermal eddy momentum flux:

$$\overline{F}_T = -\frac{1}{a\cos\phi} \frac{\partial}{\partial\phi} (\overline{v'\Phi'_z}\cos\phi) - \frac{1}{p} \frac{\partial}{\partial z} p \overline{w'\Phi'_z},$$

where

a	=	radius of the earth
ϕ	=	latitude
z	=	altitude
p	=	pressure
u'	=	perturbation westerly velocity
v'	=	perturbation northerly velocity
w'	=	perturbation vertical velocity
Φ'_z	=	perturbation geopotential

Miyahara (1978) has investigated the deposition of mean momentum and heat in the lower thermosphere connected with the dissipating (1, 1) and (2, 4) tidal modes using the above equations. In Figure 13 Miyahara's calculation of F_u and the resulting mean zonal wind are illustrated.

The (1, 1) mode is apparently capable of producing an easterly jet (~ 60 m sec^{-1}) in the equatorial lower thermosphere, and a westerly flow of order 30 m sec^{-1} at midlatitudes. Results for the (2, 4) mode in Figure 14 indicate mean zonal winds of order 10-15 m sec^{-1}, which are smaller but not negligible compared with the (1, 1) mode. The zonal flow generated by the dissipating tidal modes is comparable to the flow generated by direct solar heating in this altitude regime as computed by Dickinson *et al* (1975).

Recent calculations by Groves and Forbes (1984) indicate that the effects of tidal heating on thermospheric temperature structure appear secondary to the influence of tidal accelerations on the zonal mean wind field of the 90-150 km region.

4. TIDAL EFFECTS ON COMPOSITION

Mayr and Harris (1977) and Forbes (1978) have investigated tidal variations in thermospheric O, O_2, N_2, Ar, He and H using models that take into account the effects of tidal temperatures, horizontal and vertical tidal winds, photo- and ion-chemistry, exospheric transport, and thermal diffussion. Hydrogen tidal variations are dominated by vertical flow due to lateral transport in the exosphere, but wind induced diffusion is the single most important process for causing deviations from diffusive equilibrium (temperature-dominated) solutions of tidal variations in O, O_2, N_2, Ar, and He in the thermosphere. The effects of ion- and photo-chemistry on the variations of O and O_2, and exospheric transport on He, are found to be of secondary or negligible importance above 120 km. Measurements of neutral composition and temperature aboard the AE-E satellite have been analyzed to determine the semidiurnal and terdiurnal variations of O, N_2, He and Ar from 145-295 km (Hedin *et al,* 1980). The semidiurnal variations of O and N_2 are illustrated in Figures 15 and 16, respectively, along with predictions from the MSIS model, the Forbes model, and the Mayr *et al* (1979) model. For O variations, the Forbes and Mayr et al models predict the overall phase and ampltitude structures quite well, with some overestimate of amplitude. Surprisingly, the empirical MSIS does not fit the measurements as well as the theoretical models. On the other hand, the MSIS model provides a much better fit to the semidiurnal amplitude of N_2 whereas the other models overestimate its amplitude. The semidiurnal phases for N_2 are adequately reproduced by Forbes and MSIS models, but the Mayr *et al* model yield phases about 2 h too late above 200 km.

It is well known that winds exert an important influence on the height and density of the F-layer peak. A pronounced example is the dynamic behavior of the nighttime Arecibo ionosphere, particularly the so-called 'midnight collapse' phenomenon, which receives its primary drive from the semidiurnal tide propagating upward from the lower atmosphere. A simulation of the Arecibo ionosphere from the model of Crary and Forbes (1984) is shown in Figure 17. The post-midnight descent (or 'collapse') of the F-layer peak is shown by these authors to be precipitated by a sudden abatement of southward winds determined by a reinforcement of the in-situ excited diurnal component, an upward propagating semidiurnal component, and a terdiurnal component which these authors conjecture to arise from ion-drag coupling between the semidiurnal wind and the diurnal component of ion drag. In addition, the bunching of contours in the bottomside F-region as illustrated in Figure 17 is due to the vertical shear of the semidiurnal wind field, and may produce electron density gradients sufficient to excite the ExB gradient drift instability.

REFERENCES

Crary, D. J. and J. M. Forbes (1984), The Dynamic Ionosphere over Arecibo, A Theoretical Investigation, submitted to *J. Geophys. Res.*

Dickinson, R. E., Ridley, E. C., and Roble, R. G. (1975), Meridional Circulation in the Thermosphere, *J. Atmos. Sci. 32,* 1737-1735.

Forbes, J. M. (1979), Tidal variations in Thermospheric O, O_2, N_2, Ar, He and H, *J. Geophys. Res. 83,* 3691-3698.

Forbes, J. M. (1982), Atmospheric Tides. I, Model Description and Results for the Solar Diurnal Component. *J. Geophys. Res. 37,* 5222-5240.

Forbes, J. M. (1982), Atmospheric Tides. II. The Solar and Lunar Semidiurnal Components, *J. Geophys. Res. 37,* 5241-5252.

Garrett, H. B., and J. M. Forbes (1978), Tidal Structure of the Thermosphere at Equinox, *J. Atmos. Terr. Phys. 40,* 657-668.

Groves, G. V., and J. M. Forbes (1984), Equinox Tidal Heating of the Upper Atmosphere, *Plant. Space. Sci. 32,* 447-456.

Hedin, A. E., Spencer, N. W., and Mayr, H. G. (1980), The Semidiurnal and Terdiurnal Tides in the Equatorial Thermosphere from AE-E Measurements, *J. Geophys. Res. 85,* 1787-1791.

Mayr, H. G., Harris, I. (1977), Diurnal Variations in the Thermosphere -2. Temperature, Composition, Winds, *J. Geophys. Res. 82,* 2628-1640.

Mayr, H. G., Harris, I., Spencer, N. W., Hedin, A. E., Wharton, L. E., Porter, H. S., Walker, J. C. G., and Carlson, H. C. (1979), Atmospheric Tides and the Midnight Temperature Anomaly, *Geophys. Res. Lett. 6,* 447-450.

Miyahara, S. (1978), Zonal Mean Winds induced by Vertically Propagating Atmospheric Tidal Waves in the Lower Thermosphere, *J. Meteor. Soc. Japan 56,* 36-98.
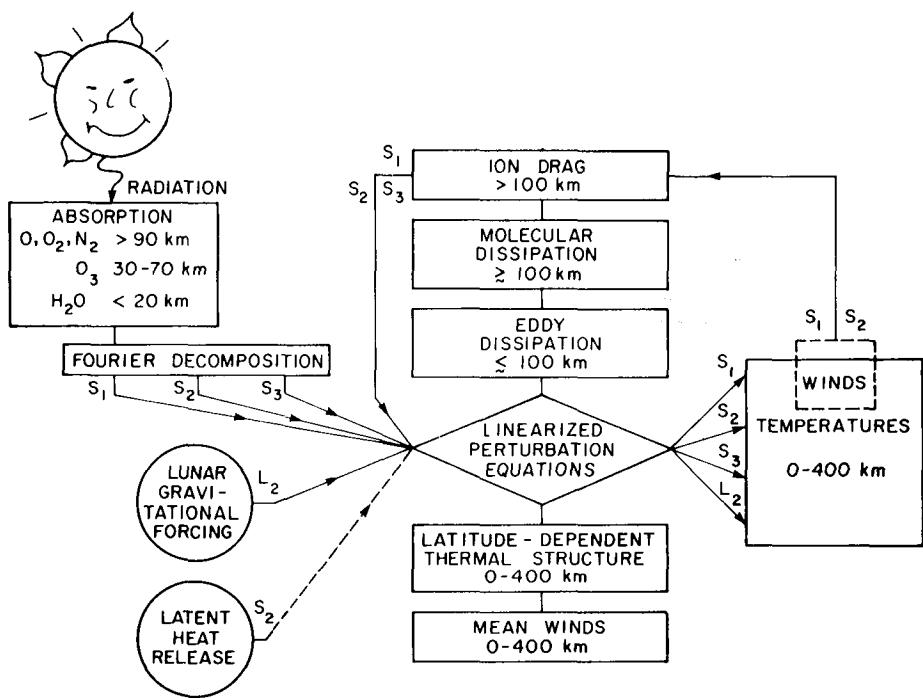
Figure 1. Schematic describing the numerical model of atmospheric tides developed by Forbes (1982 a, b).
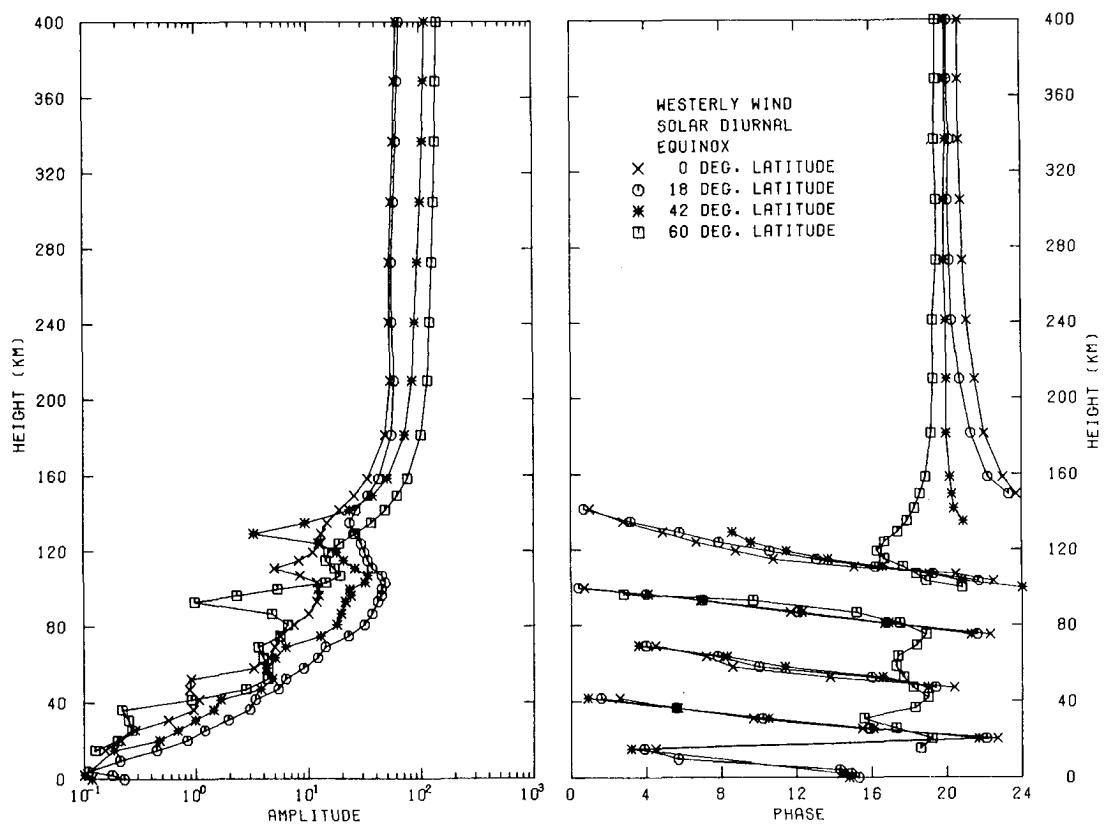
Figure 2. Diurnal westerly winds from the Forbes (1982 a, b) model.
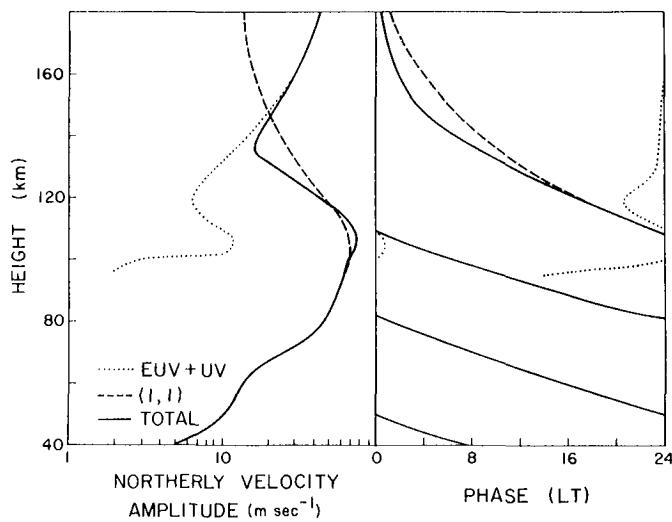
Figure 3. Northerly velocity at 18° latitude due to in situ excitation, the propagating (1, 1) Mode, and the sum of these components.
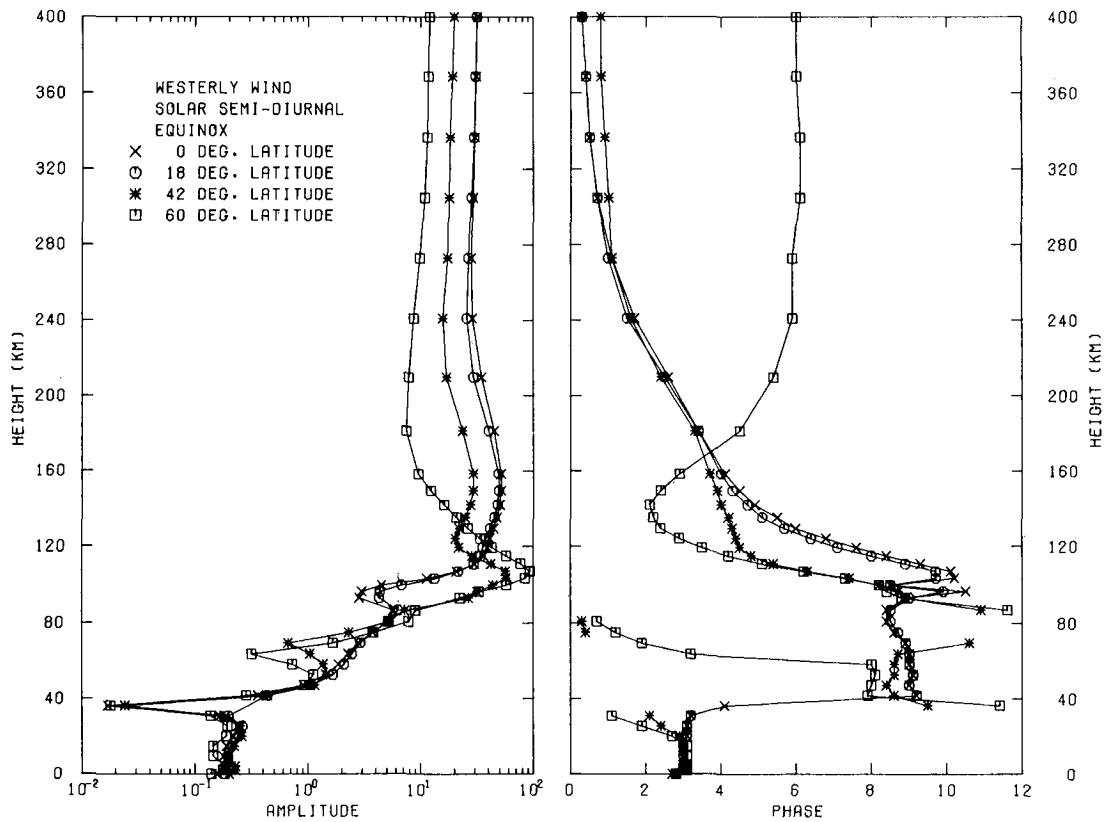
Figure 4. Solar semidiurnal westerly winds from the Forbes (1982 a, b) model.
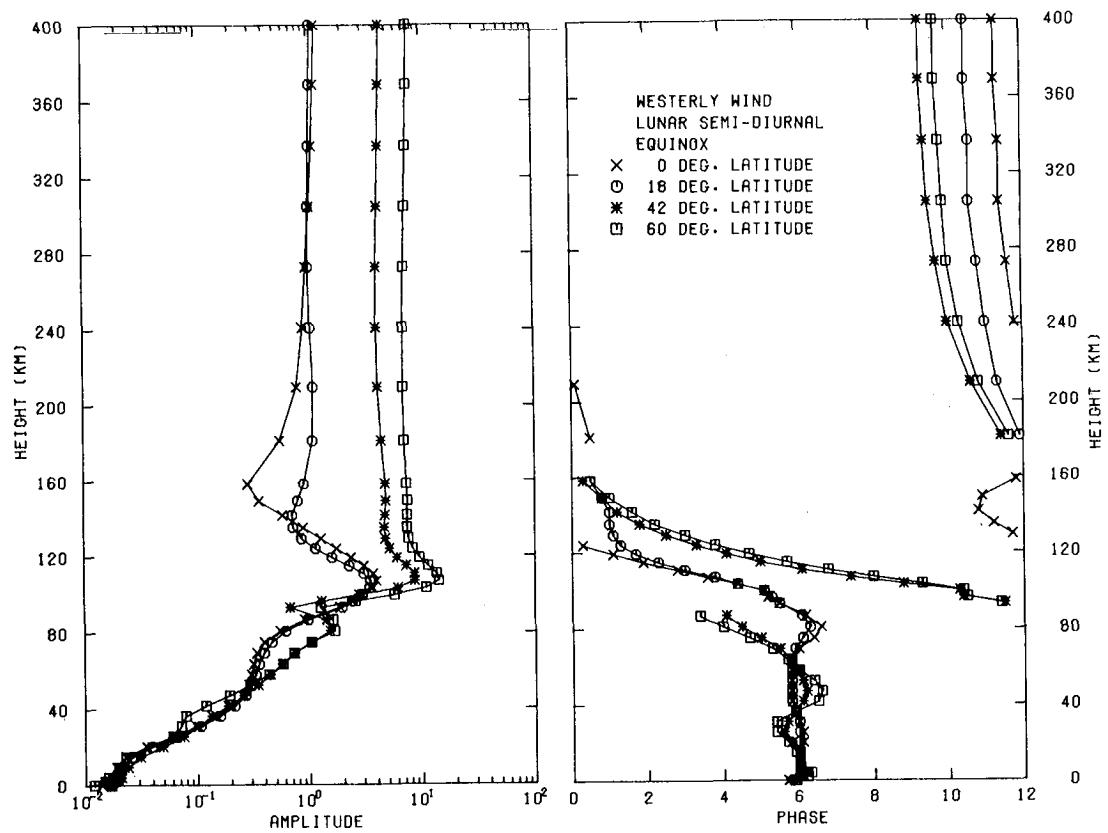
Figure 5. Lunar semidiurnal westerly winds from the Forbes (1982 a, b) model.
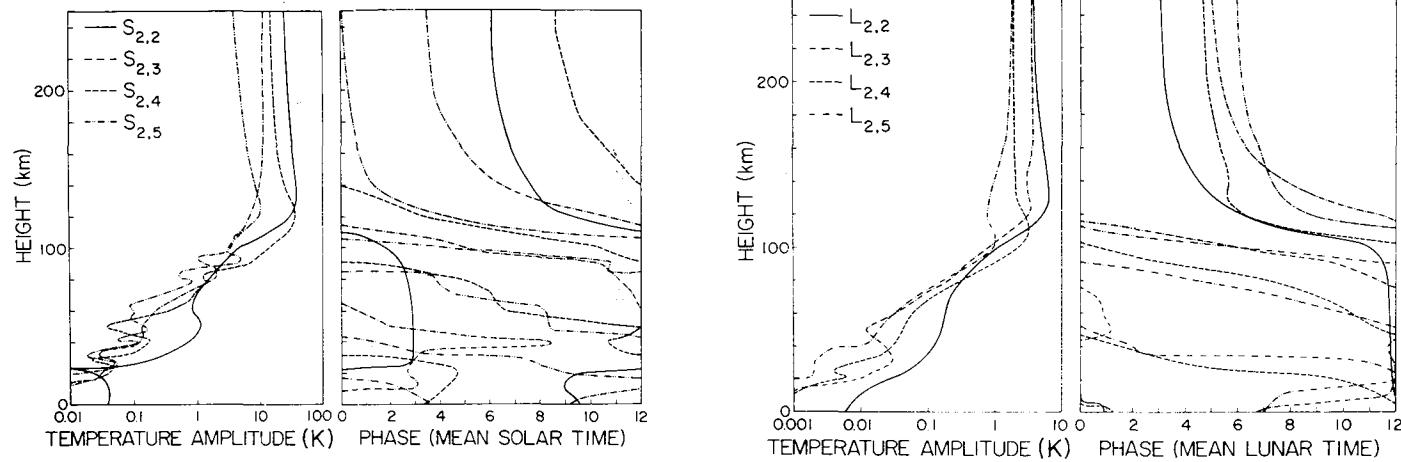
Figure 6. Hough mode decompositions of solar and lunar semidiurnal temperatures excited in the lower thermosphere.
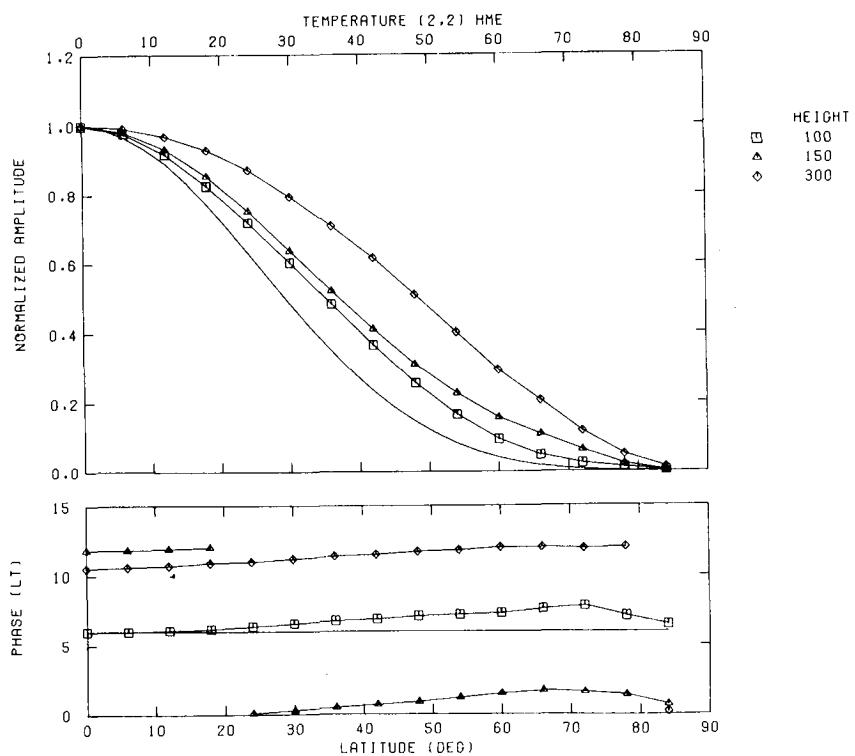
Figure 7. Normalized temperature oscillation amplitude and phase vertical structures of the (2, 2) Hough Mode Extension at 100, 150, and 300 km for $T_o = 1000$ K with normalizing factors equal to 1.00, 7.00, and 4.87, respectively.
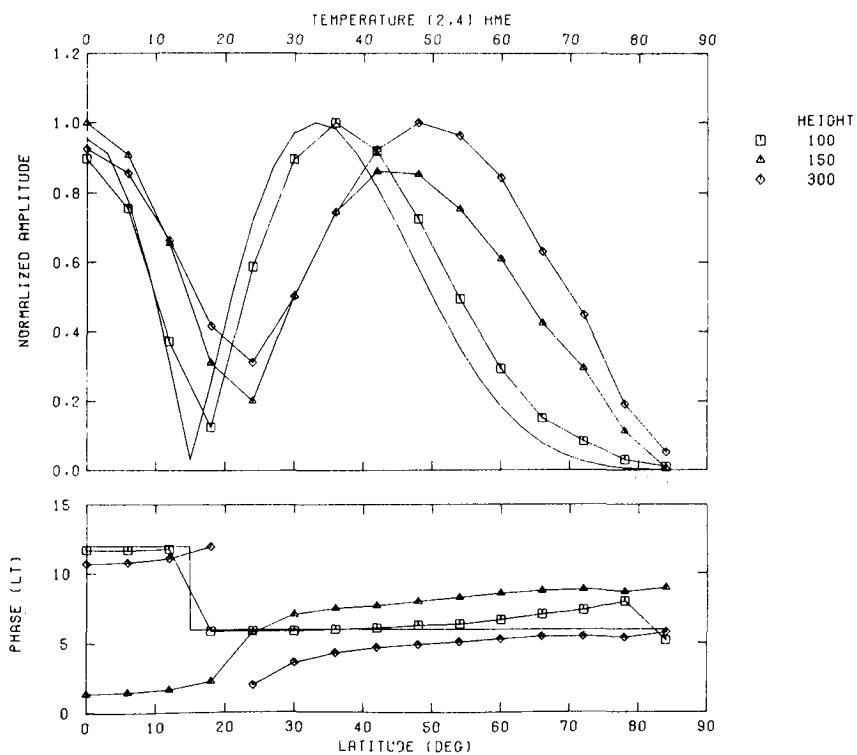
Figure 8. Normalized temperature oscillation amplitude and phase
vertical structures of the (2, 4) Hough Mode Extension at 100,
150, and 300 km, for T_o = 1000 K with normalizing factors equal
to 1.00, 2.91 and 1.88, respectively.
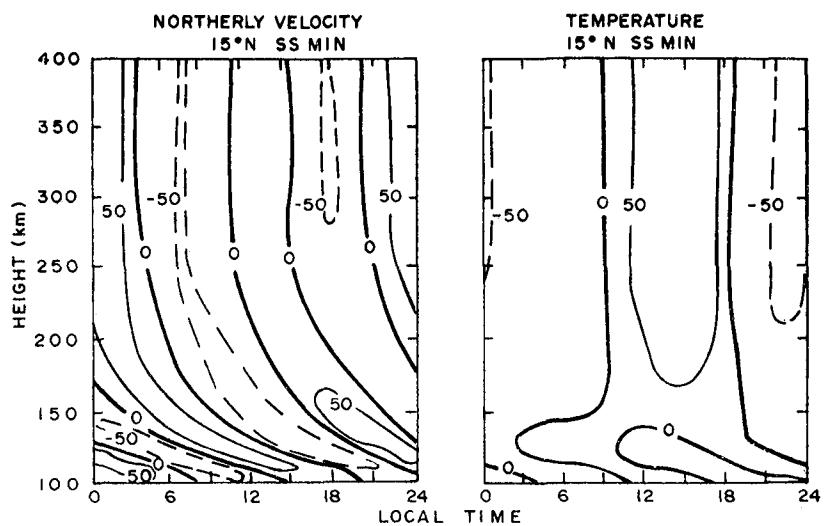
Figure 9. Wind and temperature contours from the model of
Garrett and Forbes (1978).
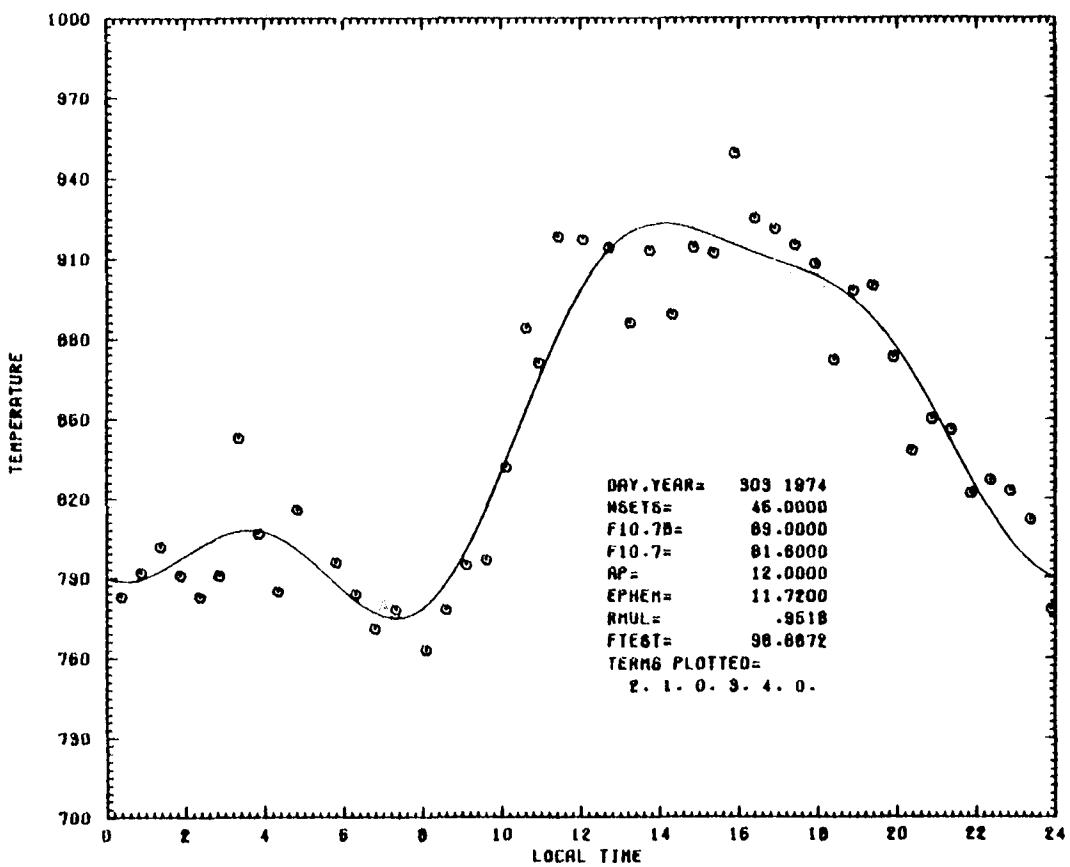
Figure 10. Example of Millstone Hill neutral exospheric temperature data during a
magnetically quiet day at solar minimum.
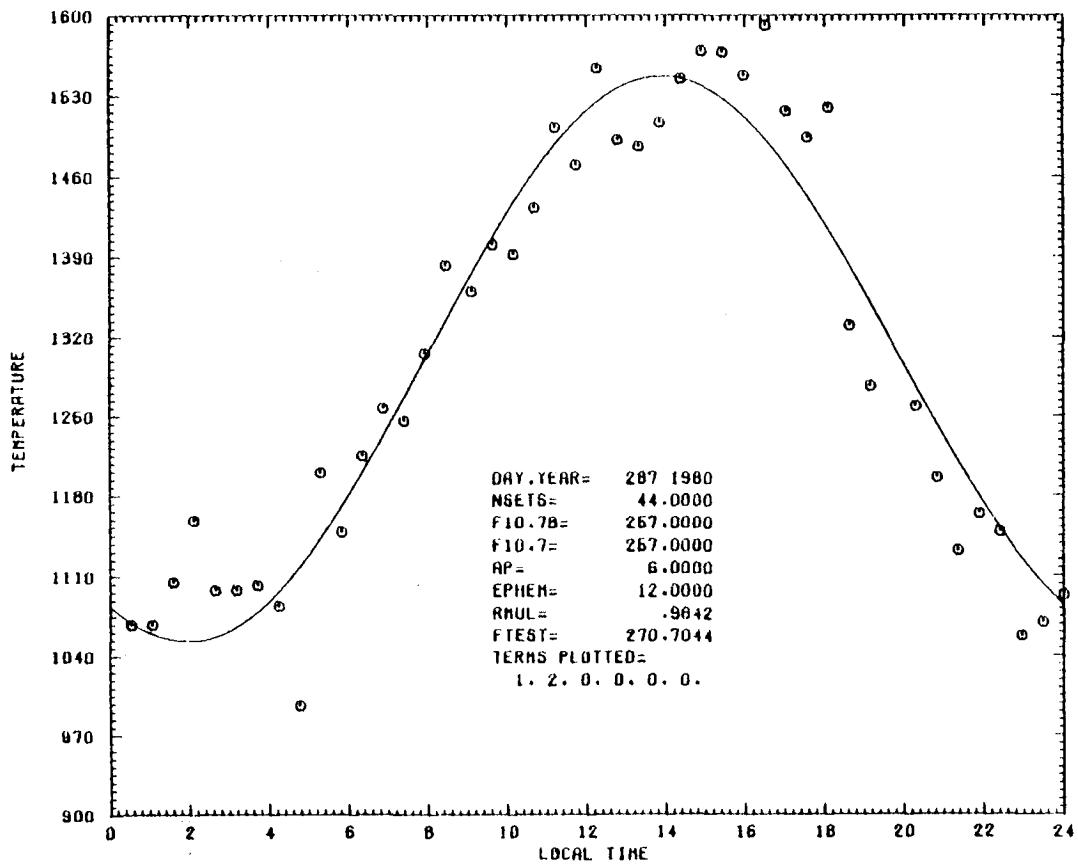
Figure 11. Example of Millstone Hill Neutral Exospheric Temperature Data During a Magnetically Quiet Day at Solar Maximum.

92
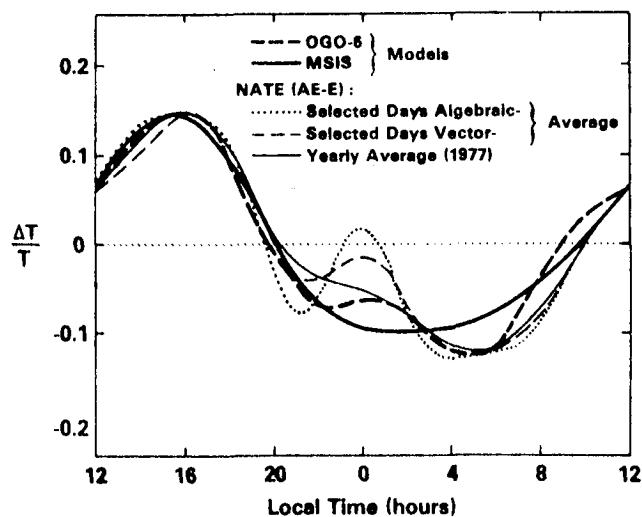
Figure 12. Comparisons between OGO-6 and
MSIS models at 250 km and fourier analyzed in-
Situ T_g measurements from the NATE
experiment on AE-E (Mayr, et al., 1979).
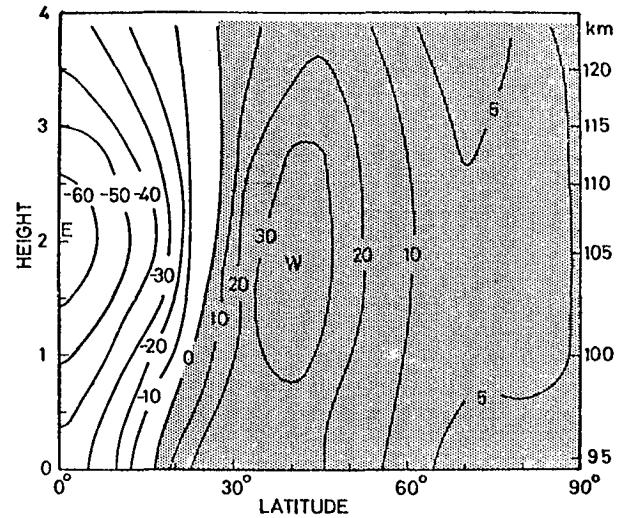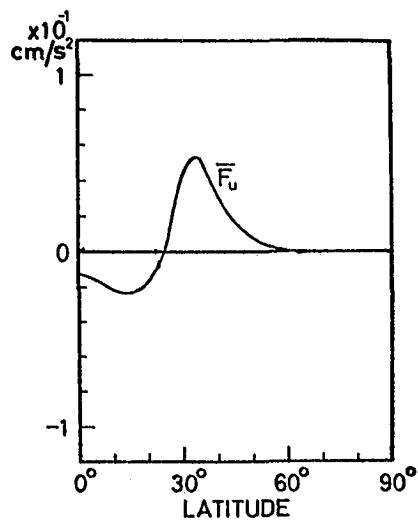
Figure 13. Divergence of eddy momentum flux (F_u) and zonal mean wind due to (1, 1) tidal mode (Miyahara, 1978).
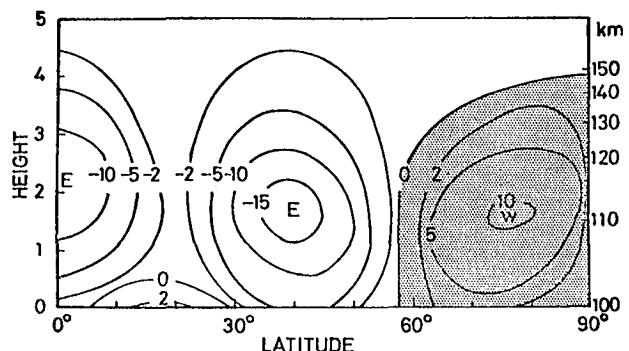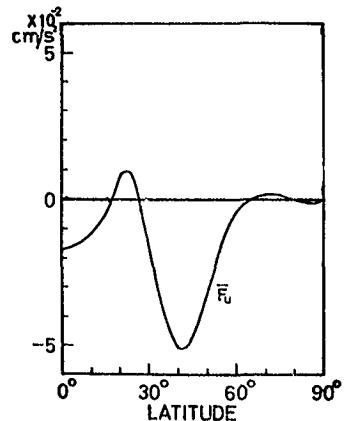
Figure 14. Divergence of eddy momentum flux (F_u) and zonal mean wind due to (2, 4) Mode. (Miyahara, 1978).

94
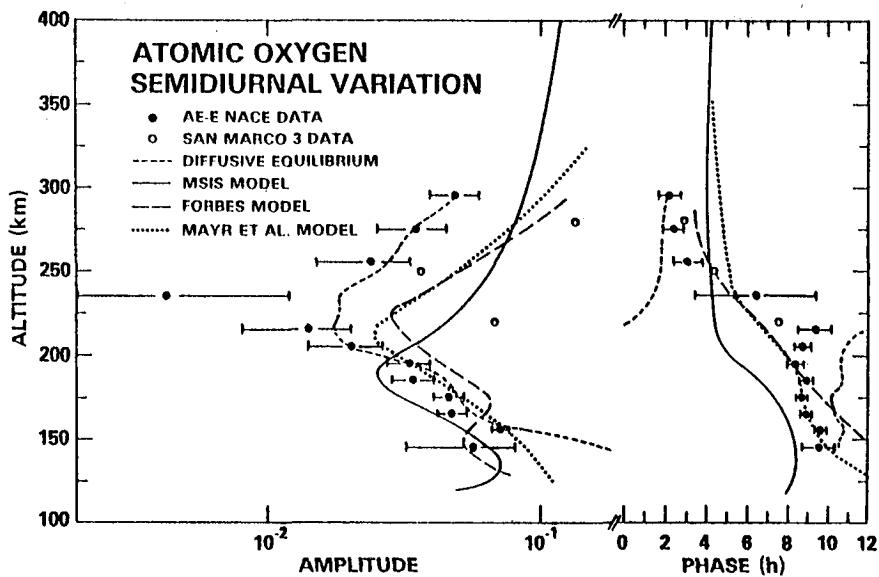
Figure 15. Atomic oxygen semidiurnal variations (Hedin, et al., 1980)
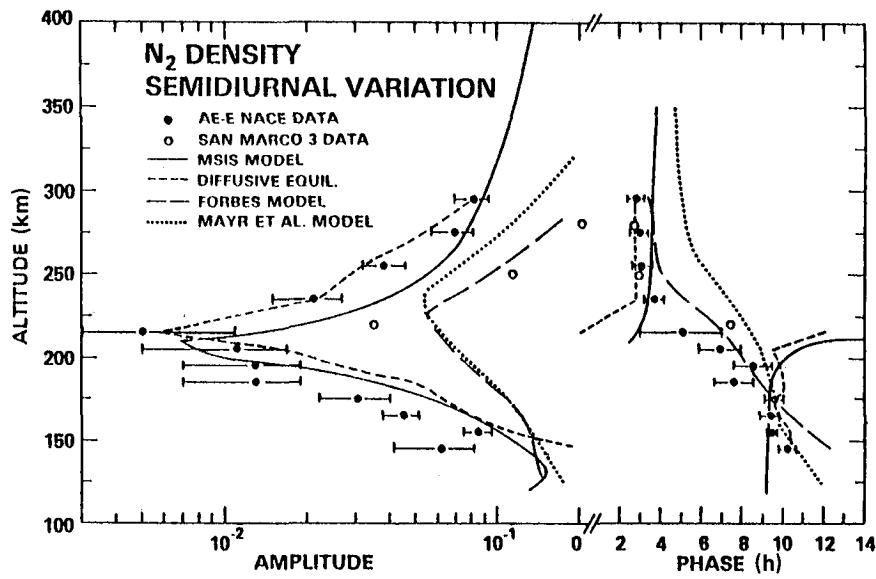
Figure 16. Molecular nitrogen semidiurnal variations (Hedin, et al., 1980).
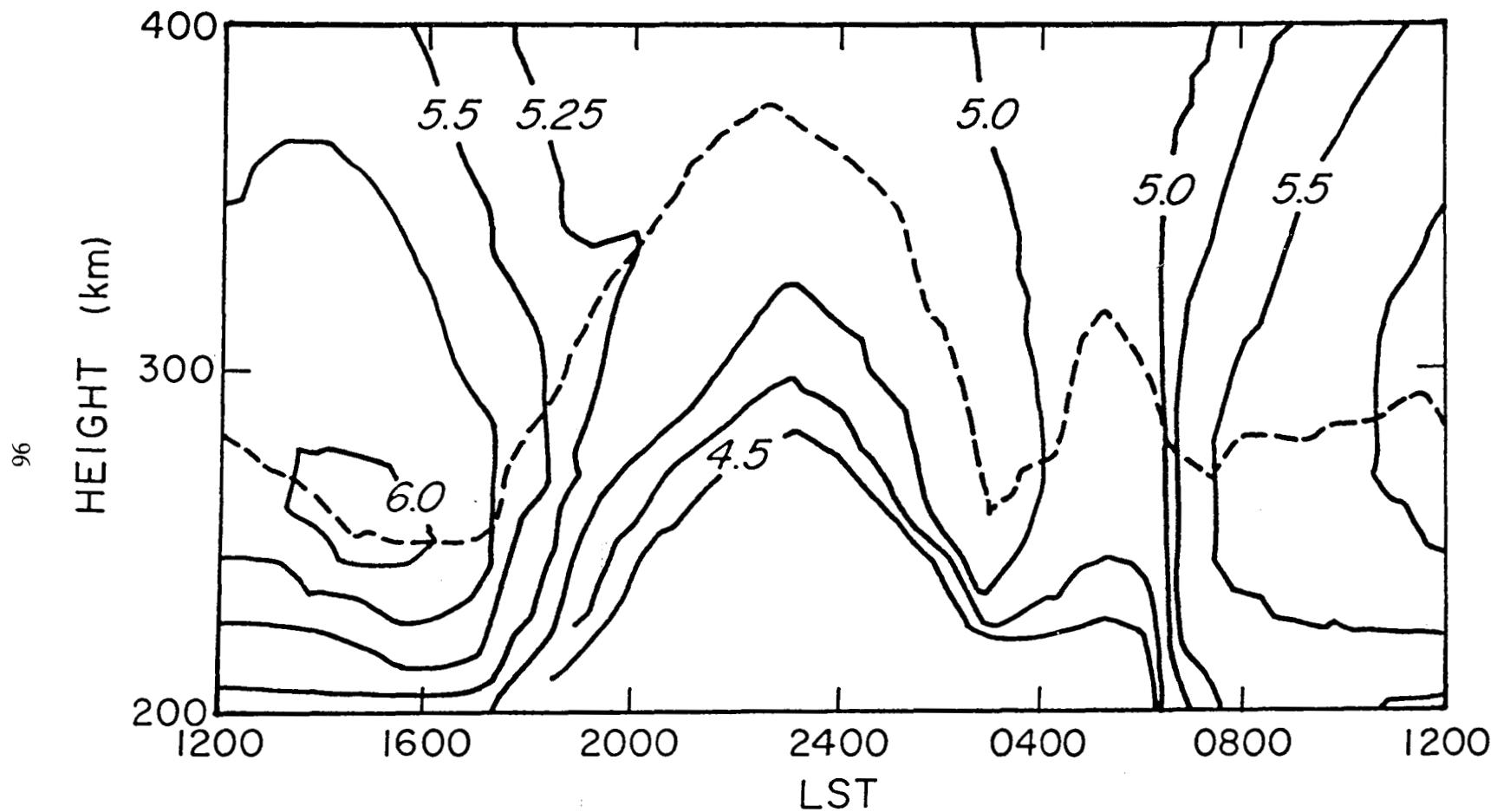
Figure 17. Log electron density contours and height of F-layer maximum density (dashed line) simulated for equinox conditions over Arecibo using the model of Crary and Forbes (1984).